J. Synchrotron Rad. (1999). **6**, 1115–1119

Paris–Edinburgh large-volume cell coupled with a fast imaging-plate system for structural investigation at high pressure and high temperature

M. Mezouar,* T. Le Bihan, H. Libotte, Y. Le Godec and D. Häusermann

European Synchrotron Radiation Facility, BP 220, 38000 Grenoble, France.
E-mail: mezouar@esrf.fr

(*Received 7 December 1998; accepted 4 August 1999*)

A new set-up for collecting high-quality data suitable for structural refinement at high pressure and high temperature has been developed on beamline ID30 at the ESRF. The possibility of using high X-ray energies, high brilliance of third-generation sources and a new fast imaging-plate detector interfaced to the Paris–Edinburgh large-volume press has lead to a significant reduction of acquisition time and improvement of the quality of the data. The feasibility of angle-dispersive X-ray diffraction experiments at high pressure and high temperature, even on light elements, has been demonstrated.

Keywords: high pressure; high temperature; Paris–Edinburgh cell; image plates; Rietveld refinement; InSb; BN.

1. Introduction

X-ray powder diffraction experiments at high pressure and high temperature are of great interest in different domains of research such as material science or geophysics. However, the quality of the information on the crystal structure and its evolution under high pressure is limited by several experimental factors: pressure gradients, preferred orientations due to imperfect sample re-crystallization, X-ray sources and detecting systems. The Paris–Edinburgh large-volume cell (Besson *et al.*, 1992) has demonstrated its capability to generate hydrostatic pressure and low-temperature gradients (Mezouar, 1997; Besson *et al.*, 1996) and is commonly used on several synchrotron sources, in energy-dispersive X-ray diffraction mode (EDX), for precise determination of PT phase diagrams (Grima *et al.*, 1995; Mezouar *et al.*, 1996). However, for full structural refinement (Rietveld refinement; Rietveld, 1969), which needs accurate determination of the diffraction intensities, the use of EDX is restricted. Indeed, the diffracted signal needs, in that case, to be corrected for the energy dependence of the brilliance of the X-ray source, response of the detector and absorption of the sample. Moreover, the single-point detector used in EDX mode intercepts only a small part of the diffracted signal and cannot take into account preferred orientations in the sample which are often present at high pressure.

Angle-dispersive X-ray diffraction (ADX) with monochromatic beam and image-plate system, which provides a large surface of detection, high resolution and wide dynamic range, represents an important alternative. This detecting system has already been successfully interfaced to diamond anvil cells (Shimomura *et al.*, 1992; Nelmes *et al.*, 1992) and to large-volume cells (Chen *et al.*, 1997, 1998). However, an important limitation, mentioned by Chen *et al.* (1997, 1998), is the large acquisition time needed for generating an exploitable image. This limitation has recently been overcome by the use of a new on-line fast imaging-plate detector (Thoms *et al.*, 1998) and the high brilliance of third-generation sources. This paper is dedicated to a detailed description of this new set-up for structural investigation at high pressure and high temperature installed on the high-pressure beamline ID30 at the ESRF. Two examples have been selected to illustrate the potential of this new device: the high-pressure and high-temperature behaviour of indium antimonide (high-Z compound) and boron nitride (low-Z compound).

2. Experimental method

2.1. *The large-volume Paris–Edinburgh press in ADX mode*

A schematic view of the high-pressure beamline ID30 at the European Synchrotron Radiation Facility (ESRF) in large-volume configuration is presented in Fig. 1. The Paris–Edinburgh press is mounted on an x-y-z translation stage which allows very precise positioning relative to the incident beam (within 1 μm). Monochromatic X-ray beams with wavelengths down to $\lambda = 0.15$ Å ($E = 100$ keV) are selected using a Si(111) channel-cut monochromator and collimated down to $50 \times 50\ \mu m^2$ by two sets of tungsten carbide slits. The precise alignment of the sample relative to the beam is performed in monochromatic mode by monitoring the X-ray absorption signal, using a silicon photodiode located between the Paris–Edinburgh press and the

detector. This photodiode is mounted on a translation stage and can be positioned in the X-ray beam at any time during the experiment. In particular, this device allows a rapid checking (<2 min) of the alignment after each compression or heating of the sample. Angle-dispersive data are collected using image plates mounted on the new *fastscan* detector (Thoms *et al.*, 1998). This new detector allows the collection of high-quality data in less than 1 min, which is at least one order of magnitude faster than other imaging-plate systems. The sample-to-detector distance is precisely determined using the diffraction pattern from a silicon powder located at the sample position. The diffraction images are corrected for spatial distortions and the portion of the Debye–Scherrer rings are integrated using the soft-

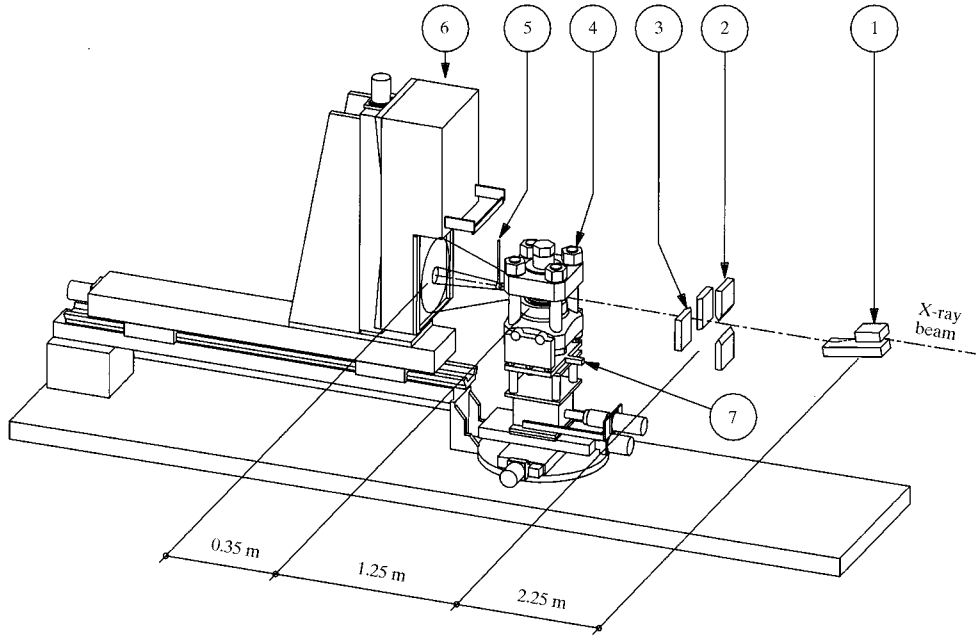

Figure 1
Layout of the high-pressure beamline ID30 at the European Synchrotron Radiation Facility (ESRF) in large-volume press configuration. 1: Si(111) channel-cut monochromator; 2–3: tungsten carbide slits, horizontal and vertical limits; 4: Paris–Edinburgh large-volume press; 5: beam stop; 6: fast-scan detector.

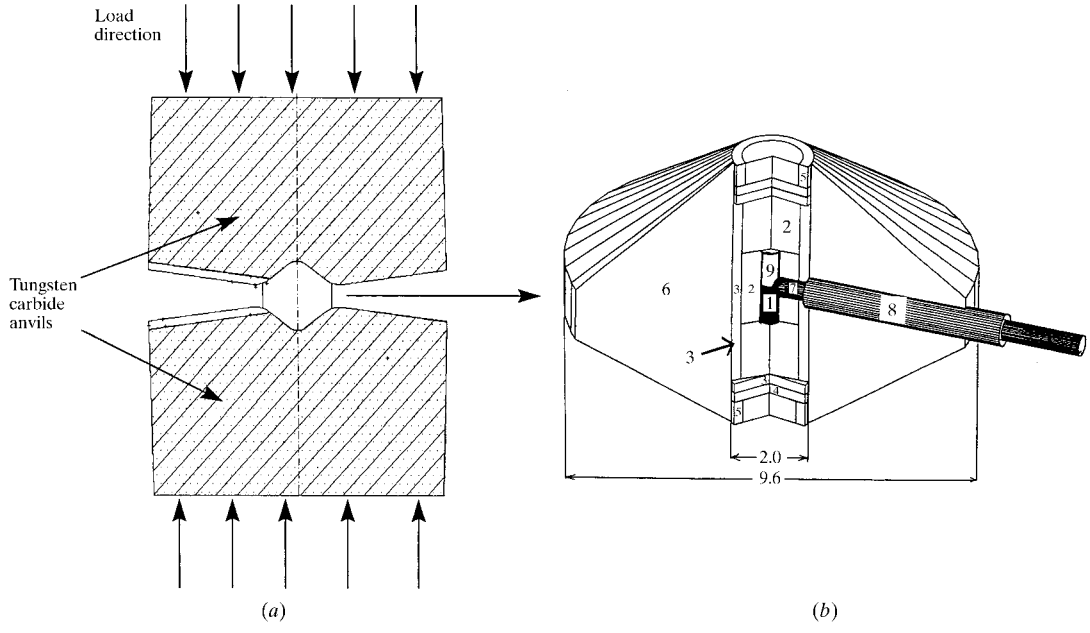

Figure 2
(*a*) High-pressure chamber. (*b*) Sample assembly. Cutaway view of the sample assembly between conoidal anvils (dimensions are in mm). 1: Sample; 2: boron nitride capsule; 3: high-resistivity graphite furnace, 4: molybdenum foil; 5: stainless-steel electrical feedthrough; 6: boron-epoxy (5:1) insulator gasket; 7: swaged chromel-alumel thermocouple; 8: ceramic sheath; 9: pressure calibrant

ware package *Fit2D* (Hammersley, 1997). Structural analyses are performed by full Rietveld refinement using the program *GSAS* (Larson & Dreele, 1994).

2.2. *Sample environment*

The sample assembly presented in Fig. 2 is contained between two supported tungsten carbide anvils with a quasi-conical profile which insures quasi-hydrostatic conditions (Makarenko, 1995) and a wide opening angle of 15°. The powder sample of height 2 mm and diameter 0.5 mm is encapsulated in a hexagonal boron nitride (h-BN) cylinder which is used as a pressure-transmitting medium. Temperatures up to 1900 K are generated by a graphite heater which is placed between the anvils and controlled by a thermocouple located at the centre of the sample assembly. In the present work a *K*-type (chromel-alumel) thermocouple was used to measure a maximum temperature of T = 1000 K. The position of the thermocouple inside the sample assembly was precisely determined using the X-ray transmission signal monitored by the silicon based photodiode. A minimum distance of 300 μm was fixed between the thermocouple tips and the X-ray beam to prevent diffraction from it. Boron-epoxy (5:1 in mass) was used as the compressing medium between the anvils. The pressure was measured *in situ* from the variation of the cell dimensions of NaCl powder as an internal calibrant, and calculated from the equation of state of Decker (1971). The location of the pressure calibrant in the sample assembly depends on the type of experiment. In the present work, in order to avoid additional peaks in the diffraction patterns, the NaCl pressure standard was positioned above the sample with an h-BN spacer in between. For each pressure–temperature (*PT*) point investigated, a diffraction image of the pressure calibrant was collected by slightly moving down the Paris–Edinburgh press. An efficient water-cooling system mounted on the tungsten carbide anvils was used to reduce the variation of the pressure on heating to less than 2% at the maximum temperature.

3. Method

3.1. *High-Z compounds*

To illustrate the potential of this new set-up we have investigated the high-pressure high-temperature behaviour of indium antimonide. Among the III–V semiconductors, indium antimonide has been one of the most extensively studied experimentally (Jayaraman *et al.*, 1961; Minomura *et al.*, 1966; McWhan & Marezio, 1966; Vanderborgh *et al.*, 1989; Nelmes *et al.*, 1993; Nelmes & McMahon, 1996) and theoretically (Zhang & Cohen, 1987; Guo *et al.*, 1993) under variable pressure and temperature. However, significant uncertainties remain in its high-pressure phase diagram. According to Mezouar *et al.* (1996), in the *PT* region defined in Fig. 3, InSb exhibits three solid modifications. At ambient conditions, InSb has the zinc blende-type structure and transforms under pressure to a metallic phase. The corresponding structure has been determined as orthorhombic with space group *Cmcm* (Nelmes *et al.*, 1993). The pressure–temperature domain of stability of this solid phase is noted IV in Fig. 3. At high temperature, another solid–solid phase transition (domain III in Fig. 3) has been firstly detected by resistivity measurements (Banus & Lavine, 1969) and numerous X-ray diffraction experiments have been performed. However, the data available on the crystal structure of this solid phase are still conflicting. Indeed, Banus & Lavine (1969) have determined the structure as tetragonal with space group $I4_1/amd$, whereas this phase has been identified as orthorhombic with space

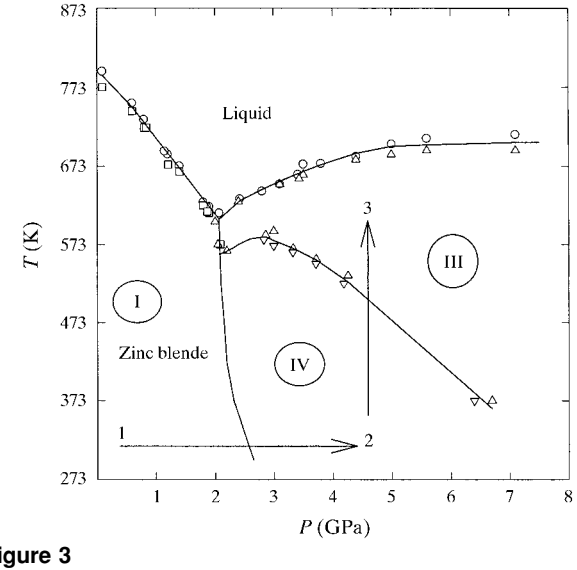

Figure 3
Phase diagram of InSb according to Mezouar *et al.* (1996). The thermodynamic path followed in this work: 1, ambient conditions; 2, P = 4.7 GPa, T = 373 K; 3, P = 4.7 GPa, T = 623 K.

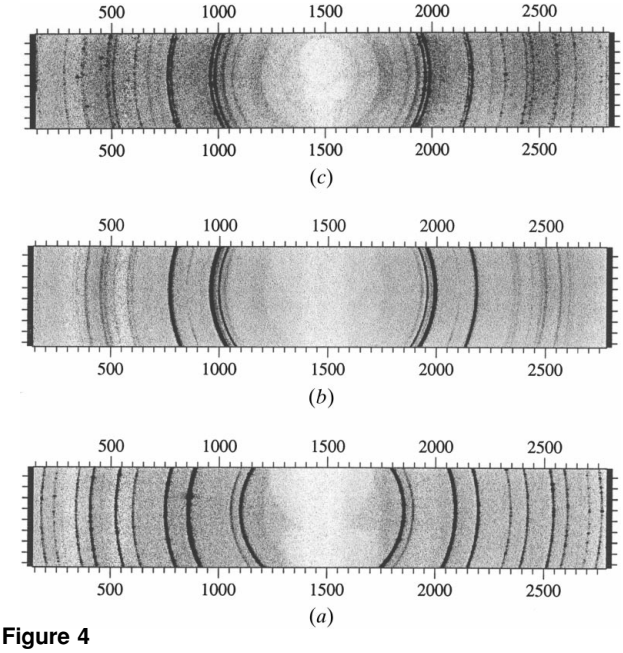

Figure 4
ADX diffraction patterns of the high-pressure high-temperature phase of InSb. (*a*) Position 1 in Fig. 3. (*b*) Position 2 in Fig. 3. (*c*) Position 3 in Fig. 3.

group *Pmmm* or *Pmmn* by Yu *et al.* (1978), and orthorhombic with space group *Immm* by Mezouar *et al.* (1996) and Nelmes & McMahon (1996).

In the present study we have re-examined the structure of solid III (*i.e.* corresponding to domain III in Fig. 3) *in situ* using our angle-dispersive powder diffraction set-up. The optimum wavelength in terms of contrast between the sample and its environment, and photon flux, was found at $\lambda = 0.1494$ Å. Indeed, for the high-Z compounds like InSb, the large difference in scattering power between the sample and its surroundings (boron gasket, graphite heater, h-BN capsule) increases strongly with the X-ray energy. At 83 keV the extra peaks from the sample environment indicated by asterisks in Fig. 5 are very weak and can be neglected. To reach the PT domain of the phase III, the pressure was slowly increased at room temperature in steps of 0.1 GPa from the solid I to the pure solid IV. At this point the temperature was raised carefully in steps of 10 K up to the pure solid III (*i.e.* free from solid IV). At each PT point the evolution of the diffraction pattern was checked in order to follow structural changes in real time. The sequence of transitions is shown in Figs. 4(*a*), 4(*b*) and 4(*c*). The transition from solid IV to solid III is accompanied by significant changes: the number of diffraction peaks decreases strongly which indicates a transition to a structure with higher symmetry. The diffraction pattern in Fig. 4(*c*) presents more spotty Debye–Scherrer rings due to recrystallization effects near the melting curve.

The data were of sufficient quality to allow us to clearly identify the crystal structure of the solid III as tetragonal with space group $I\bar{4}m2$ (β-tin-type structure) and to perform a full structural refinement. Several other space groups have been tested. In particular, all the previously proposed symmetries (I_{41}/amd, *Pmmm*, *Pmmn*, *Immm*) have been tried, and exhibit important deviations from the observed profile. The variables in the refinement were the lattice parameters a and c, a scale factor, three peak-shape parameters, an isotropic thermal motion parameter and a preferred orientation parameter. The result is presented in Fig. 5 and shows that the agreement between observed and calculated profiles is excellent. Indeed, the R_{wp} factor ($R_{wp} = \{\Sigma w_i[y_i(\text{obs}) - y_i(\text{calc})]^2/\Sigma w_i[y_i(\text{obs})]^2\}^{1/2}$) and the $R_F{}^2$ factor [$R_F{}^2 = \Sigma|F_{hkl}(\text{obs})^2 - F_{hkl}(\text{calc})^2|/F_{hkl}(\text{obs})^2$] which represent the deviation from the observed intensities and structure factors, respectively, became 0.05 and 0.04. The refined cell parameters are $a = b = 5.7462 \pm 0.0003$ Å and $c = 3.1434 \pm 0.0003$ Å at $P = 4.7$ GPa and $T = 603$ K

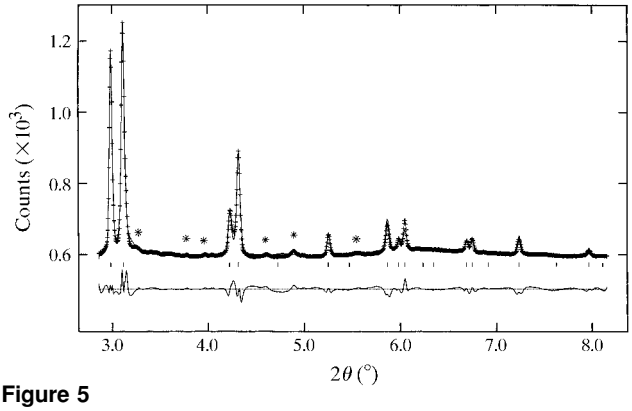

Figure 5
Rietveld refinement of a disordered β-tin structure (space group $I\bar{4}m2$) to the integrated profile of InSb obtained at $P = 4.7$ GPa and $T = 603$ K. The tick marks under the profile indicate the reflections allowed for this space group. Asterisks: contamination peaks from the sample environment.

3.2. *Low-Z compounds*

As described in §2.2, the sample environment is mainly composed of boron and carbon which have a low X-ray scattering power. However, for low-Z samples the extraction of the diffracted signal still remains difficult because, in that case, scattered signals coming from the surrounding material and from the sample are of the same order of magnitude. The subtraction method used to solve this problem is illustrated in Fig. 6. The selected example concerns the rhombohedral phase of boron nitride (space group $R3m$) which is a metastable solid modification of this compound. The sample consists of a powder of CVD-produced bulk pyrolytic r-BN, having a density of 2.26 g cm^{-3} and containing less than 5% volume of h-BN impurities. In order to avoid chemical reaction between the h-BN capsule and r-BN, the sample was pre-compacted and loaded directly into the graphite heater. The wavelength was fixed at $\lambda = 0.2232$ Å, and the pressure and temperature conditions of the experiment were $P = 5$ GPa and $T = 573$ K. Fig. 6 shows diffraction patterns from the sample and its surroundings, and of the surroundings only, taken by slightly translating the press in the direction perpendicular to the X-ray beam. The signal from the sample is extracted by subtracting these two diffraction patterns, after scaling. The corresponding two-dimensional images have been obtained in only 30 s. This exposure time was selected to fully use the dynamic range (14 bits) of the image plate. The

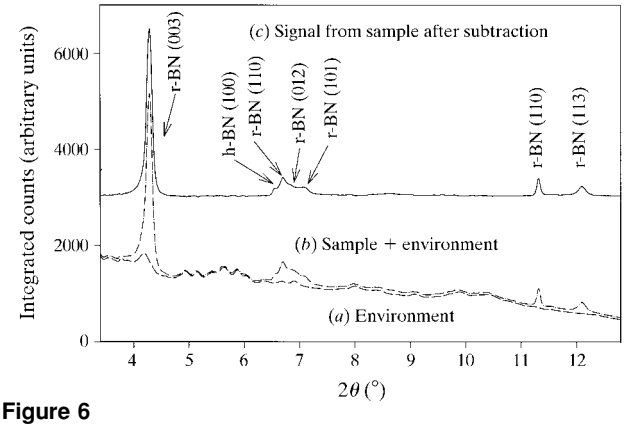

Figure 6
Integrated spectra of rhombohedral boron nitride (r-BN). (*a*) r-BN and the pressure medium at 5 GPa and 2473 K; (*b*) only the pressure medium close to the sample; (*c*) final spectrum of the sample after subtraction of the sample environment. The corresponding images were collected in 30 s using 55.5 keV radiation. Miller indices (*hkl*) of the r-BN sample and h-BN impurities are indicated.

quality of subtraction has been improved by the use of high-energy photons (E = 55.5 keV) which considerably limit the self-absorption by the sample. The refined cell parameters of r-BN at P = 5 GPa and T = 473 K are a = 2.493 ± 0.001 Å and c = 9.135 ± 0.001 Å. They have been determined by fitting the diffraction peaks positions to a pseudo-Voigt function using the program *Fit2D*.

4. Conclusions

A fast imaging plate is interfaced to a Paris–Edinburgh press for the rapid collection of *in situ* X-ray powder diffraction data suitable for structural refinement at high pressure and high temperature. Indeed, this is the first large-volume press mounted on a third-generation synchrotron source. Moreover, this set-up is interfaced to a fast on-line detector, which is at least ten times faster than other imaging-plate systems. This new set-up allows structural phase transformations to be followed very precisely over a wide range of pressure and temperature, and several experiments have already been successfully performed. The structure of InSb III has been unambiguously determined and the feasibility of ADX experiments, even on light elements, has been demonstrated.

We are grateful to Stany Bauchau for his technical help. One of the authors (HL) would like to thank J. P. Gaspard from the University of Liege for all support provided during his stay at the ESRF.

References

Banus, M. D. & Lavine, M. C. (1969). *J. Appl. Phys.* **40**, 409–413.
Besson, J. M., Grima, P., Gauthier, M., Itié, J. P., Mezouar, M., Häusermann, D. & Hanfland, M. (1996). *Phys. Status Solidi B*, **198**, 419–425.
Besson, J. M., Nelmes, R. J., Hamel, G., Loveday, J. S., Weill, G. & Hull, S. (1992). *Physica B*, **180/181**, 907–913.
Chen, J., Kikegawa, T., Shimomura, O. & Iwasaki, H. (1997). *J. Synchrotron Rad.* **4**, 21–27.
Chen, J., Parise, J. B., Li, R., Weidner, D. J. & Vaughan, M. (1998). *Properties of Earth and Planetary Materials at High Pressure and Temperature, Geophysical Monograph 101*, edited by M. H. Manghani & T. Yagi, pp. 139–144. Washington DC: AGU.
Decker, D. L. (1971). *J. Appl. Phys.* **42**, 3239–3243.
Grima, P., Polian, A., Gauthier, M., Itié, J. P., Mezouar, M., Weill, G. & Besson, J. M. (1995). *J. Chem. Solids*, **56**, 525–530.
Guo, G. Y., Crain, J., Blaha, P. & Temmerman, W. M. (1993). *Phys. Rev. B*, **47**(9), 4841.
Hammersley, A. (1997). *Fit2D*. ESRF, Grenoble, France.
Jayaraman, A., Newton, R. C. & Kennedy, G. C. (1961). *Nature (London)*, **191**, 1290–1291.
Larson, A. & Von Dreele, B. (1994). *GSAS*. Los Alamos Laboratory, Los Alamos, NM 87545, USA.
Makarenko, I. (1995). Private communication.
McWhan, D. B. & Marezio, M. (1966). *J. Chem. Phys.* **45**(7), 2508–2511.
Mezouar, M. (1997). PhD thesis, Université Denis Diderot Paris VII, France.
Mezouar, M., Besson, J. M., Syfosse, G., Itié, J. P., Häusermann, D. & Hanfland, M. (1996). *Phys. Status Solidi B*, **198**, 403–410.
Minomura, S., Okai, B., Nagasaki, H. & Tanuma, I. (1966). *Phys. Lett.* **21**(3), 272–273.
Nelmes, R. J., Hatton, P. D., McMahon, M. I., Piltz, R. O., Crain, J., Cernik, R. J. & Bushnell-Wye, G. (1992). *Rev. Sci. Instrum.* **63**, 1039–1043.
Nelmes, R. J. & McMahon, M. I. (1996). *Phys. Rev. Lett.* **77**, 663–666.
Nelmes, R. J., McMahon, M. I., Hatton, P. D., Crain, J. & Piltz, R. O. (1993). *Phys. Rev. B*, **47**, 35–54.
Rietveld, H. M. (1969). *J. Appl. Cryst.* **2**, 65–71.
Shimomura, O., Takemura, K., Fujihisa, H., Fujii, Y., Ohishi, Y., Kikegawa, T., Amemiya, Y. & Matsushita, T. (1992). *Rev. Sci. Instrum.* **63**, 967–971.
Thoms, M., Bauchau, S., Kunz, M., Le Bihan, T., Mezouar, M., Häusermann, D. & Strawbridge, D. (1998). *Nucl. Instrum. Methods*, A**413**, 175–180.
Vanderborgh, C. A., Vohra, Y. K. & Ruoff, A. L. (1989). *Phys. Rev. B*, **40**(18), 12450–12456.
Yu, S. C., Spain, I. L. & Skelton, E. F. (1978). *J. Appl. Phys.* **49**(9), 4741–4745.
Zhang, S. B. & Cohen, M. L. (1987). *Phys. Rev. B*, **35**(14), 7604–7610.